TECHNICAL MEMORANDUM

826

Use of in situ observations to verify the diurnal cycle of sea surface temperature in ECMWF coupled model forecasts

D. Salisbury, K. Mogensen & G. Balsamo

Research Department

November 2018

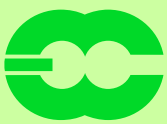

European Centre for Medium-Range Weather Forecasts
Europäisches Zentrum für mittelfristige Wettervorhersage
Centre européen pour les prévisions météorologiques à moyen terme

Series: ECMWF Technical Memoranda

A full list of ECMWF Publications can be found on our web site under:
http://www.ecmwf.int/en/research/publications

Contact: library@ecmwf.int

European Centre for Medium-Range Weather Forecasts
Shinfield Park, Reading, RG2 9AX, England

Abstract

At the European Centre for Medium-Range Weather Forecasts (ECMWF), coupling of the atmospheric model to an ocean model has recently been extended to the High-Resolution (HRES) forecast model. This move is driven by: (i) encouraging results in coupled Ensemble medium-range and extended-range forecasts; (ii) studies reporting a positive impact of coupling on the prediction of atmospheric events; and (iii) the need to better represent coupling feedbacks. As the lower atmospheric boundary condition over the ocean for the atmospheric model, the sea surface temperature (SST) field is key to this coupling. It is known that sub-daily variation in SST—its diurnal cycle—modulates air-sea exchange at the interface, and that resolving this variation can have a positive impact on the forecasting of both the upper ocean and the atmospheric state. In this work, we explore the diurnal cycle of SST in global coupled simulations with the ECMWF Integrated Forecast System (IFS). A year's worth (March 1, 2015–March 1, 2016) of 10-day forecasts are run under coupled and then uncoupled model configurations: in the uncoupled runs, the (at depth) SST is based on the daily Operational Sea Surface Temperature and Sea Ice Analysis (OSTIA) field, with use of a prognostic scheme for the skin surface temperature; in the coupled runs the atmospheric model is coupled to the NEMO ocean model with a one-hour coupling frequency. The amplitude and phase of the diurnal cycle are validated against estimates from in situ oceanographic observations. We also explore the dependencies of the modelled diurnal cycle on key meteorological forcings (10-m wind speed and total cloud cover), and compare with the dependencies exhibited by the observations.

1 Introduction

Sea surface temperature (SST) is a key parameter for weather and climate due to its influence on the state and evolution of the Earth's atmosphere—via atmosphere-ocean interactions—and on ocean dynamics. Accurate SST data are a requirement for climate monitoring, prediction, and research. In addition, measurements or estimates of SST are used in the retrieval of other key ocean and atmosphere parameters from in situ and satellite-based instruments. SST has an important impact on the biogeochemistry of the ocean and is one of the most important physical properties of the marine ecosystem.

One dominant mode of variation in SST is its diurnal variability. The daily progression of solar heating and subsequent surface- or mixing-driven cooling of the upper ocean is known as the diurnal cycle of SST. The diurnal cycle is an important feature of atmosphere-ocean interaction as many physical exchanges, including those of sensible and latent heat, and trace gases, are sensitive to the temperature of the ocean surface and its variation. For example, large diurnal warming can increase the heat flux from the ocean by 50–60 Wm^{-2} during the daytime (Ward, 2006; Fairall et al., 1996). Using data from moored buoys in the tropical Pacific, Zeng and Dickinson (1998) showed evidence of clear diurnal variability in surface latent and sensible heat fluxes. This variability could not be reproduced using daily or monthly mean sea surface skin temperature, $\mathrm{SST}_{\mathrm{skin}}$, suggesting that the diurnal cycle of skin temperature is the main driver of flux diurnal variability.

Atmospheric General Circulation Models (AGCMs) often use as input SST analysis fields representing a bulk or foundation SST, constructed from satellite and in situ SST observations. Prognostic and diagnostic schemes are typically used to represent diurnal SST variation (Fairall et al., 1996; Stuart-Menteth, 2003; Webster et al., 1996; Zeng and Beljaars, 2005; Takaya et al., 2010a; Filipiak et al., 2012) in the absence of an ocean model. Alternatively, the diurnal cycle of SST can be reproduced using an ocean-atmosphere coupled model with a short coupling interval, of roughly 1–3 hours, as long as the ocean component can adequately resolve the near-surface thermal structure. This approach has been used to assess the impact of the diurnal cycle on the atmosphere on sub-daily to intraseasonal timescales. Bernie et al. (2007) used a diurnally-forced ocean GCM to investigate the impact of resolving the diurnal cycle

on the SST response to the Madden–Julian Oscillation (MJO). Across the Indo-Pacific, the diurnal cycle has been shown to increase the intraseasonal SST response to the MJO by around 20%. The diurnal cycle also modifies momentum exchange between currents, resulting in a 10% increase in the strength of Ekman cells and equatorial upwelling. In the second part of the study, Bernie et al. (2008) investigated the impact of a resolved ocean diurnal cycle on the climate simulations of a coupled GCM, showing that inclusion of the diurnal cycle leads to increase of the mean SST, with an increase of 0.2–0.3°C across the equatorial Pacific. In turn, these changes had profound impact on up-scale variability in the tropical climate. Other studies have linked the diurnal cycle of SST to convection over the Tropical Pacific (Johnson et al., 1999), to the diurnal cycle of precipitation (Dai and Trenberth, 2004), and shown that the SST diurnal cycle modulates the mean climate of atmospheric models (Brunke et al., 2008).

In numerical weather prediction, coupled models traditionally show good skill in seasonal and monthly prediction, in particular in forecasting SST, the MJO, and the prediction of hurricanes and cyclones (Brassington et al., 2015). It is thought that part of this success is due to inclusion of diurnal SST variability, and that the increase in forecast skill could be seen in short- and medium-range forecasts, given the variable nature of air-sea interaction on even hourly time scales. McLay et al. (2012) report that inclusion of SST variation in the Navy Operational Global Atmospheric Prediction System improves medium-range forecast skill in the tropics, with a smaller impact in the midlatitudes. In the tropics, most of the increased skill was due to SST analysis perturbations rather than from inclusion of diurnal variability.

The move to coupled forecasting systems at ECMWF is driven by improvement in the modelling of air-sea interaction processes, the development of ocean-atmosphere coupled data analysis, and use of coupled wave-sea-ice-atmosphere forecasts at all time ranges. Atmosphere-ocean coupling has recently been extended to the High-Resolution (HRES) forecast model (cycle 45r1). In preparation for such a move, it is important to quantify how well the diurnal cycle is represented in the coupled simulations.

This study aims to verify the diurnal cycle in a coupled implementation of the ECMWF IFS model, and compare with results from an uncoupled implementation. The amplitude and phase of the diurnal cycle are validated against estimates from in situ oceanographic observations. We also explore the dependency of the modelled and observed diurnal cycle amplitude on key meteorological forcings of diurnal variability in SST—the 10-m wind speed and total cloud cover. In Section 2 we give an overview of the diurnal cycle and its representation in the ECMWF model. Model experiments and data are described in Section 3, and the methodology is outlined in Section 4. Results are given in Section 5, followed by discussion (Section 6) and conclusions (Section 7).

2 Background

2.1 Definition and measurement of sea surface temperatures

Traditionally, the sea surface temperature observed from ships and buoys is reported as the "bulk" SST—the temperature at a depth of roughly 1 m or deeper (Donlon et al., 2007). Note that the Global Ocean Data Assimilation Experiment (GODAE) High-Resolution SST Pilot Project (GHRSST-PP) Science Team recommends using SST_{depth} rather than "bulk" SST; this is to avoid confusion relating to potential drastic changes in the bulk temperature with depth, and to encourage reporting of the depth of the temperature measurement.

SST_{bulk} can differ markedly from the skin temperature (SST_{skin}) of the water in the top several microns

of depth. As the atmosphere senses only the interface of the ocean, SST_{skin} is of great importance as it represents the temperature closest to that of the interface. The skin temperature can be measured by in situ- or satellite-based radiometric instruments, although substantive effort is involved in quality control of the observations.

Under most oceanographic and meteorological conditions, SST_{skin} is greater than a bulk temperature at depth, and shows larger diurnal variation due to the decrease in solar heating of the ocean surface boundary layer with depth. However, during the night, or under strong winds and with wave-induced mixing, the two temperatures can show little difference. Indeed, under such conditions—i.e., in the absence of a diurnal thermocline—SST_{skin} can be lower than SST_{bulk} due to the cool-skin effect (Fairall et al., 1996).

The foundation temperature of the ocean, SST_{fnd}, is defined as the the temperature of the water column free of diurnal temperature variability. It is the temperature from which the growth of the diurnal thermocline develops each day.

2.2 The diurnal cycle of SST

Under calm conditions and with the onset of shortwave radiative heating during the early morning, the top few metres of the ocean warm; about half of the incoming energy is absorbed within the upper meter (Soloviev et al., 2013). This net heating results in a stably stratified layer called the "diurnal warm layer". The temperature cycle peaks in the early afternoon (circa 2pm local time), before solar insolation reduces during the afternoon, and the warm layer begins to deepen due to turbulent mixing, leading to a decrease in SST. During the night, surface-driven cooling leads to further mixing which pushes the turbulent boundary layer to its greatest depth. The stratification that built up during the day is all but eroded, ready for the cycle to repeat again.

The magnitude of diurnal warming is determined by the competing effects of processes favouring stratification of the water column (primarily through the vertical gradient of short wave radiation absorption, but also through positive surface buoyancy fluxes) and processes leading to destabilization (wind driven-mixing, and surface evaporation and cooling). Meteorological and oceanographic factors that affect the diurnal cycle of SST therefore include (i) the net heat flux due to solar radiation (largely determined by the cloud cover), (ii) wind speed, (iii) the foundation temperature and salinity of the water, (iv) optical attenuation of the water column, and (v) processes inducing vertical mixing or stratification.

Averaged globally and over the seasons, the mean amplitude of the diurnal cycle—defined as the difference between the local daily maximum and minimum SST—is order 0.1°C (Kawai and Wada, 2007). In favourable conditions of strong solar insolation and weak winds, the amplitude can exceed 5°C (Kawai and Wada, 2007). Under enhanced wind-driven mixing the amplitude is much smaller; it has been reported that the diurnal thermocline almost disappears when wind speed exceeds 5 m s^{-1} (Soloviev and Lukas, 1997; Donlon et al., 2002), due to a combination of increased turbulent mixing in the ocean and the drawing of heat from the ocean by a more turbulent atmosphere. Given the potentially large gradient in temperature above 1-m depth in the daytime, the diurnal cycle amplitude generally decreases with depth (Kawai and Wada, 2007).

Though the diurnal variation of SST has been measured from research vessels for over a century—first by collecting water samples and then using expendable probes, buoys, profiling floats and radiometric instruments—the advent of operational satellite SST observations in the 1980s enabled measurement of SST in a globally-consistent manner. Stuart-Menteth (2003) report the first global climatological distribution of the day–night skin SST difference based on infrared measurements; the data reveal regions

that are susceptible to large diurnal warming, such as the Mediterranean Sea, the Bay of Bengal, the Arabian Sea, the seas around Japan, the north Pacific off North America, and the Azores-Bermuda high pressure belt. Subsequent studies based on satellite data confirm an increase in amplitude and decrease in seasonality towards the equator of the diurnal amplitude of SST, with a primary dependence on wind speed and solar insolation variability.

2.3 Diurnal SST variability in the ECMWF model

Atmosphere-ocean coupling was introduced in the IFS model to improve seasonal forecast skill, with specific focus on prediction of the MJO, before being extended to monthly forecasts. It was shown that ocean-atmosphere coupled predictions were superior to those made using persisted SSTs (Woolnough et al., 2007). The coupled model has since been used for the Extended-Range (monthly) and Long-Range forecasts (seasonal), as well as the Ensemble Forecast System (ENS). In the ENS, since CY40R1, coupling is now from day 0, instead of day 10 as was the case in previous cycles. Results have shown that the coupled ocean–atmosphere–wave model better forecasts the tropical atmosphere and the MJO, and has impacts on the representation of slow-moving tropical cyclones. Breivik et al. (2015) reported that the coupled integrations show reduced SST bias; this was attributed to the impact on SST of included a sea-state dependent mixing scheme. The impact of ocean coupling on tropical cyclone intensity in the Western Pacific was investigated by Mogensen et al. (2017); the impact of coupling varied from cyclone to cyclone, but the oceanic and atmospheric response to the cyclones looked physically sound.

Since September 2008 (CY35R1), the diurnal cycle of SST has been represented in the IFS through use of a prognostic scheme for SST_{skin} (Zeng and Beljaars, 2005) (ZB05). The scheme—which solves the one-dimensional heat transfer equation in the near-surface layer—parameterises both the warm layer and the cool skin. It was later refined to include the impact of Langmuir circulation on diurnal warming, and then tested against buoy observations and satellite data (Takaya et al., 2010a). Including the effects of Langmuir circulation enhanced surface layer mixing and reduced diurnal variability of SST under wavy conditions. Though the revised scheme showed better agreement with buoy SST observations than the original scheme, based on validation using buoy and satellite data it consistently under-estimated diurnal amplitudes in calm, clear-sky conditions, but over-estimated amplitudes in moderate to high winds.

The impact on medium-range forecasts of explicitly resolving the diurnal cycle in the IFS was investigated by implementing a one-dimensional mixed-layer ocean model (Takaya et al., 2010b). Though there was an overall neutral impact on forecast skill for general meteorological variables compared with an uncoupled control experiment, the mixed-layer model showed improvements of SST forecast skill particularly in the summer hemisphere at a 10-day time scale. Inclusion of the mixed-layer model also improved the prediction skill of the MJO and the Indian Monsoon in medium-range forecasts. The amplitude of the diurnal cycle from the model was compared with estimates from the ZB05 scheme. Despite its simplicity, the skin-layer scheme showed some advantage over the mixed-layer model.

3 Model experiments and data

We used the operational (at the time of writing) version (CY43R3) of the IFS with TCo1279 atmospheric resolution (grid spacing of around 9 km). The model was run in an uncoupled (with prescribed SST and sea ice fields) or coupled (i.e., with interactive ocean and sea-ice models) mode. In the uncoupled simulations, the atmosphere is forced by persisted anomalies, with initial SST from the OSTIA (Operational Sea Surface Temperature and Sea Ice Analysis) product. OSTIA is produced with global coverage (grid

spatial resolution of 1/20°) on a daily basis by the Met Office, using a blend of satellite retrievals and in situ observations from ships (Donlon et al., 2012). The analysis provides estimates for the foundation temperature SST_{fnd}.

In the uncoupled experiments, the Takaya et al. (2010a) cool-skin and warm-layer scheme is implemented in the atmospheric model. The scheme is forced by the OSTIA SST fields and provides estimates of SST_{skin}. With the scheme switched off, the resulting skin temperature is equal to the SST forcing the scheme.

The coupled configuration includes an interactive ocean, namely the NEMO model (version 3.4.1) (Madec, 2008) with ECMWF modifications to the coupling interface (Mogensen et al., 2012). The skin sea surface temperature required by the atmospheric model is obtained from the SST of the uppermost 1-m of the ocean and the cool-skin scheme of Takaya et al. (2010a) (note that the warm-layer scheme is switched off). The ocean mixing settings in NEMO for the coupled configuration are detailed by (Breivik et al., 2015). The ocean initial conditions are from OCEAN5 analysis system using the Behind-Real-Time stream (Zuo et al., 2017, 2018).

3.1 Validation data

The in situ observations used in this study comprise drifting and moored buoy measurements of SST, obtained from ECMWF's Meteorological Archival and Retrieval System (MARS), which are originally distributed via the World Meteorological Organisation (WMO)'s Global Telecommunication System (GTS). Measurements are obtained at a depth of roughly 20–30 cm, though the exact measurement depth is not recorded. Based on these observations, a set of NEMO observation operator output files in netCDF was produced for each 1-hr time step of each 10-day forecast, for each set of experiments. The files contain observations of a given set of meteorological and oceanographic variables, together with the interpolated model equivalent values valid at the observation location (specified by the reported latitude and longitude values). Files for the individual time steps are merged (to form a 10-day time series) and then split into files for individual stations based on its identifier code. Figure 1 shows time series of representative data—after basic quality control—for key variables over the 10-day forecast initialised on 01 June 2015, for station 61002 in the Mediterranean Sea.

Also included in the files are observations (if available) and model equivalent values for key meteorological and oceanographic variables including the mean sea level pressure, the 10-m wind speed, direction and their zonal and meridional components, the 2-m air temperature and dewpoint temperature, and the total cloud cover. Extra model variables (ocean current speed and components, and sea ice fraction) as well as auxiliary information for the ocean grid (land-sea mask, ocean depth, and distance to coast) are included, as are meteorological and oceanographic variables of interest (included the 10-m wind speed, air temperature, and ocean current velocity components), and key model details (such as the distance to nearest coast, and bathymetry).

4 Methodology

To validate modelled diurnal cycle of SST, we compared $dSST_{mod}$ to the corresponding observed values ($dSST_{obs}$). Though not a like-for-like comparison, this methodology makes best use of the available observations and allows investigation into the representation of the diurnal cycle of SST in the different model configurations. For each station, the diurnal cycle amplitude (dSST) and phase, along with mean

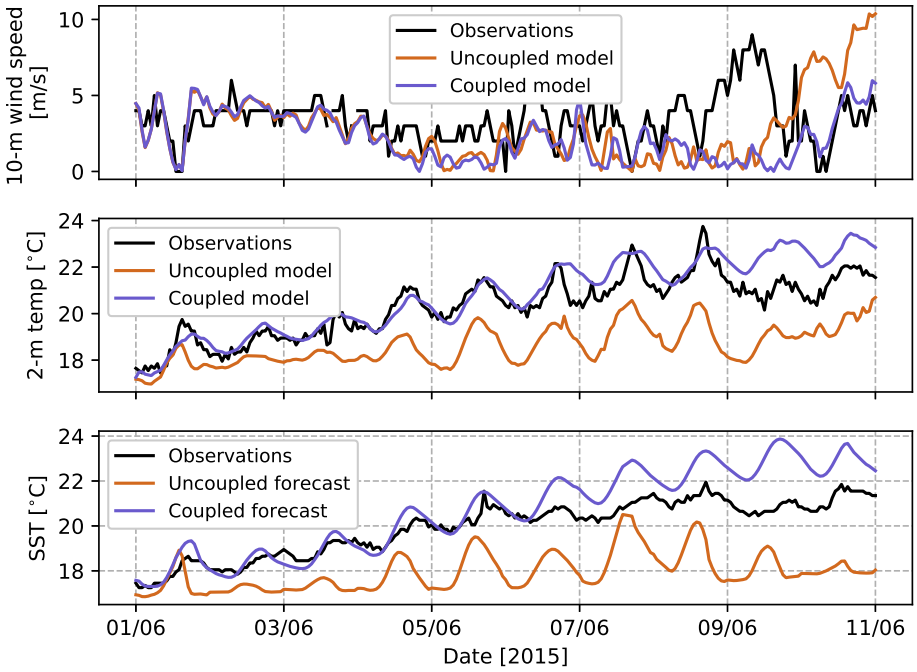

Figure 1: Time series of observed (upper panel) 10-m wind speed, (middle panel) 2-m temperature, and (bottom panel) SST for station 61002 in the Mediterranean Sea together with uncoupled model and coupled model estimates for those variables valid at the station's location, for one 10-day forecast initialised at 00 UTC, 01 June 2015.

values for all meteorological and oceanographic variables, were calculated for each day (0–24 UTC) of each forecast. The amplitude of the diurnal cycle was calculated as the maximum minus minimum SST during a forecast day: $\mathrm{dSST} = \mathrm{SST}_{\mathrm{max}} - \mathrm{SST}_{\mathrm{min}}$. The phase (Local Solar Time, LST) was determined as the time of day at which SST reaches its maximum value. The phase was calculated only if the diurnal cycle amplitude within a given 24-hr period exceeds 0.25°C.

Due to the nature of obtaining in situ observations in the marine environment, there are often gaps in the records. To ensure that data coverage issues do not bias our analysis, diurnal cycle amplitude and phase were only calculated if at least one SST observation is available in each quarter of a forecast day. To deal with spurious data, a simple quality control procedure identified unrealistic values and large jumps (3°C or larger for successive values) in the SST time series; if these jumps are found the suspect values are masked. A quality control flag on the SST observations was also used to disregard problematic data. The reported latitude and longitude values of the observations were screened for spurious values which could significantly affect estimation of the mean location of each station over a 24-hour period. The final dataset comprises order 4,775,000 model–observation estimates of diurnal cycle amplitude for each of the two sets of experiments, with use of data from around 2700 individual stations. The number of model–observation estimates of diurnal cycle phase is order 1,228,000 for uncoupled experiments, and 1,800,000 for the coupled experiments.

To aid analysis of spatial trends, data has been grouped into $2^\circ \times 2^\circ$ grid cells. The number of diurnal cycle estimates over the course of the year varies dramatically with location, due to the distribution of observations (Figure 2). Note that the grid cells are not equal-area. Regions dense with observations include the Atlantic Ocean around 30°N, and the Tropical Pacific, the latter a result of the TAO/TRITTON

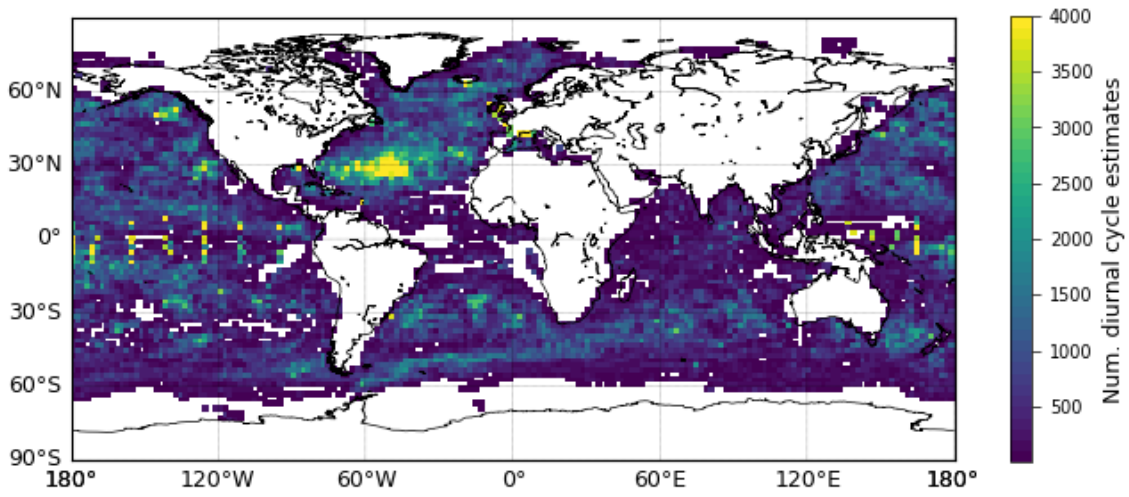

Figure 2: The number of diurnal cycle estimates in each $2^\circ \times 2^\circ$ grid box for the year of 10-day forecasts.

array moorings. Regions with sparse or no observations include the equatorial Atlantic, and the southern extra-tropics of the Pacific.

5 Results

5.1 Diurnal cycle amplitude

5.1.1 Diurnal variation in modelled and observed SST

In Figure 3 we compare $\mathrm{dSST}_{\mathrm{mod}}$ from the uncoupled (left column) and coupled (right column) simulations with $\mathrm{dSST}_{\mathrm{obs}}$, for a subset of days spanning the 10-day forecasts.

In the uncoupled forecasts, there is a general trend of underestimation of $\mathrm{dSST}_{\mathrm{mod}}$. Values of $\mathrm{dSST}_{\mathrm{mod}}$ in the uncoupled simulations rarely reach 0.5°C but can occasionally reach much larger values under favourable conditions (i.e., low wind speeds and low cloud cover), as seen in Figure 1. There is a greater degree of correlation between $\mathrm{dSST}_{\mathrm{mod}}$ and $\mathrm{dSST}_{\mathrm{obs}}$ in the coupled simulations than in the uncoupled simulations; the correlation coefficient (R) values are higher for the coupled simulations than for uncoupled simulations throughout the forecast. This higher degree of correlation for the coupled simulations is due to on average larger values of the model diurnal cycle amplitude, particularity when the observed diurnal cycle amplitude is large. In both sets of simulations there is a divergence of estimates of $\mathrm{dSST}_{\mathrm{mod}}$ and $\mathrm{dSST}_{\mathrm{obs}}$ as the forecasts progress, with R values reducing steadily from forecast day 1.

To understand these results more quantitatively, we explore the distribution of values for $\mathrm{dSST}_{\mathrm{mod}} - \mathrm{dSST}_{\mathrm{obs}}$ over the course of the forecast range. The distribution on selected forecast days for the uncoupled (left panels) and coupled (right panels) simulations are represented as histograms and shown in Figure 4. The number of model–observation matchups is indicated, along with statistics for the distributions.

For the uncoupled experiments, the distributions have a mean value of -0.10–-0.11°C and a constant median of -0.05°C. The values indicate that, on average, $\mathrm{dSST}_{\mathrm{mod}}$ is roughly a tenth of a degree smaller

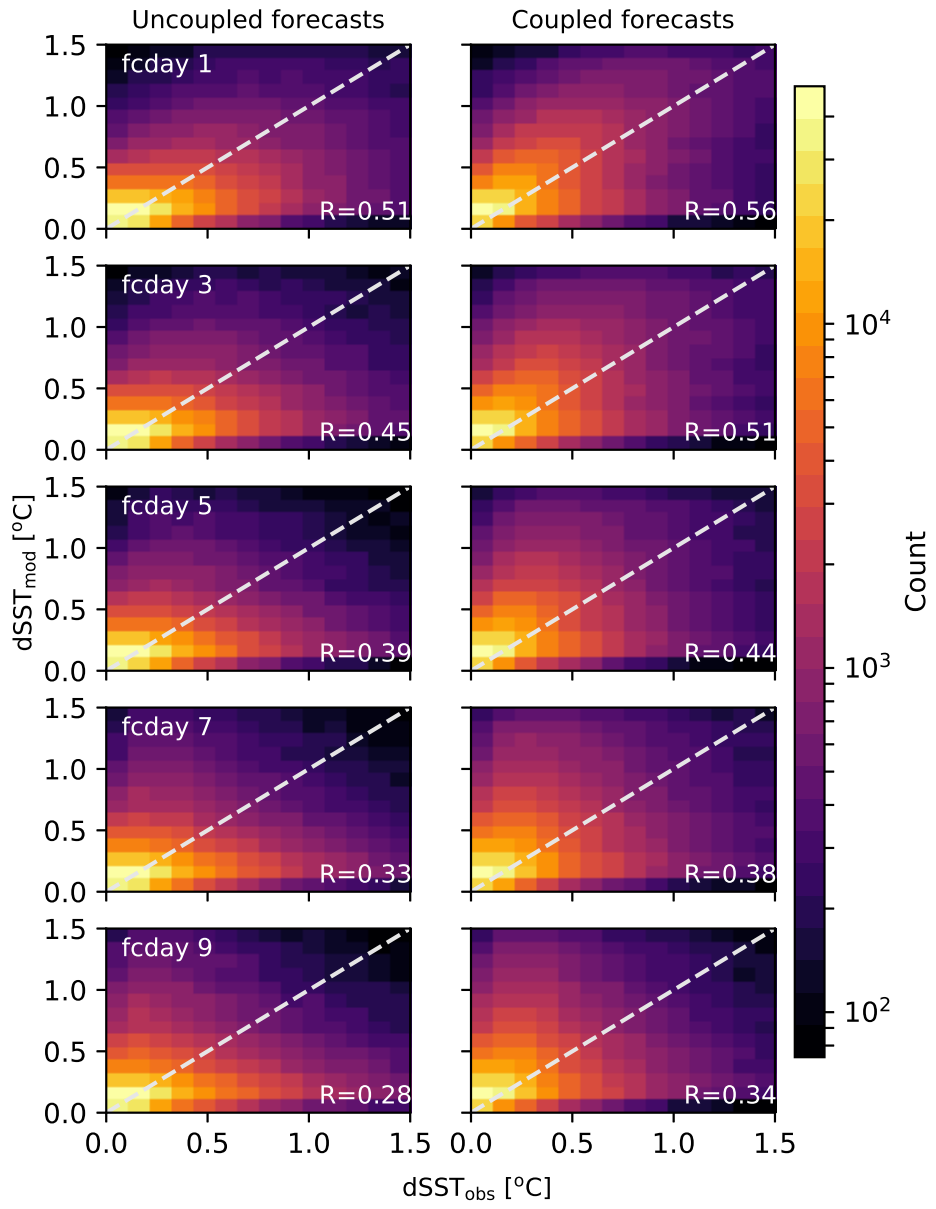

Figure 3: 2D density plots of $dSST_{obs}$ and $dSST_{mod}$ estimates on select days of the forecast validity range for (left column) uncoupled and (right column) coupled simulations.

than $dSST_{obs}$. There is a slight broadening of the distribution as the forecasts progress, with the standard deviation increasing from 0.44°C on day 0 to 0.54°C on day 9, indicating that larger differences between the two quantities are more frequent as the forecasts progress.

For the coupled simulations, the mean and median values of the distributions remain steady throughout the forecasts at close to 0°C, indicating good agreement between $dSST_{mod}$ and $dSST_{obs}$. The standard deviation of the distribution increases steadily from 0.46° on forecast day 0 to 0.54° on forecast day 9, revealing an overall slight increase in variance for the coupled simulations. The frequency of cases where the model and observed diurnal cycle amplitude show a large difference (i.e., > 1°C) is roughly equivalent between the two sets of results.

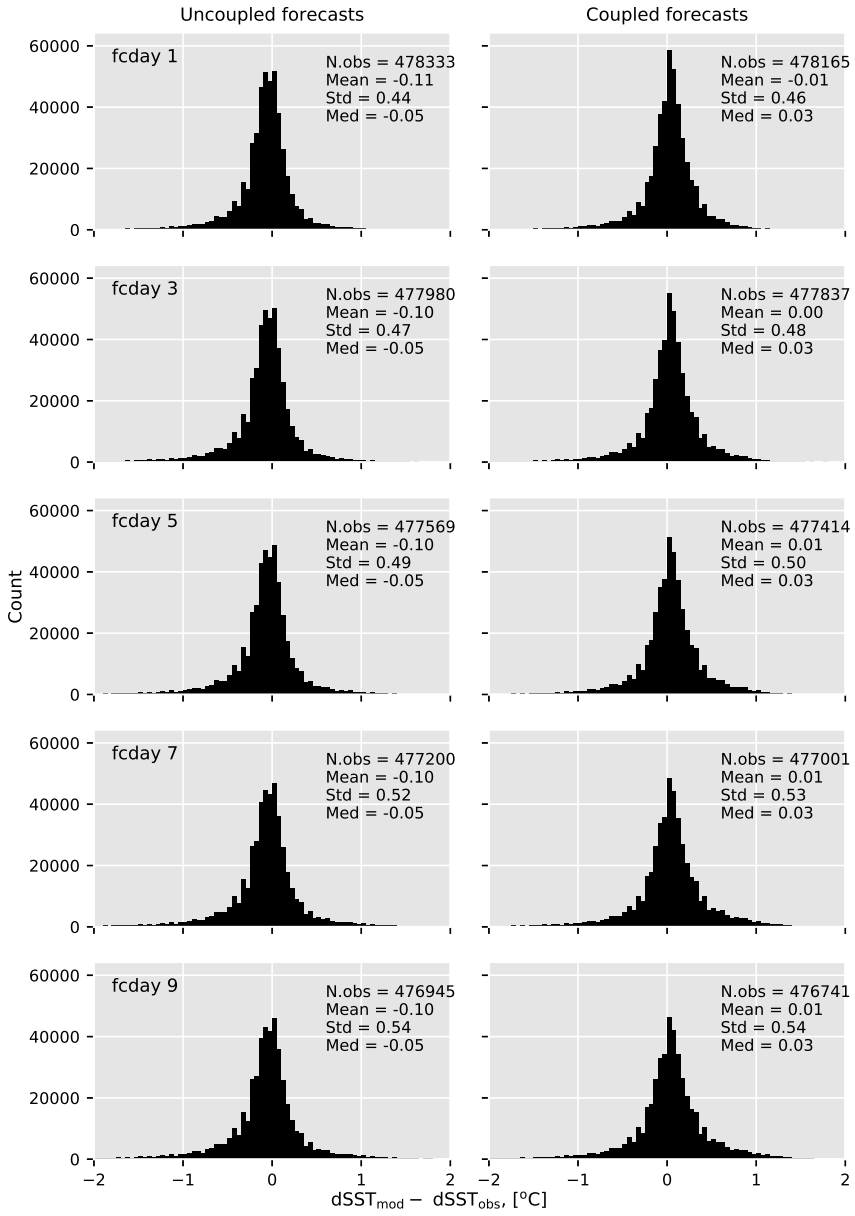

Figure 4: Histogram of $\mathrm{dSST_{mod}} - \mathrm{dSST_{obs}}$ on select days of the forecast validity range for (left column) uncoupled and (right column) coupled simulations.

5.1.2 Global geographical distribution

We next explore the geographical distribution of SST diurnal cycle amplitude estimates. The geographical distribution of the year-averaged $\mathrm{dSST_{obs}}$ (i.e., $\overline{\mathrm{dSST_{obs}}}$) is shown in panel (a) of Figure 5. Over much of the global ocean, $\overline{\mathrm{dSST_{obs}}} < 0.4°\mathrm{C}$. Many coastal regions—especially those in the tropics—have a larger diurnal cycle amplitude, with values greater than 0.8°C. Also apparent are areas with unexpectedly large values of $\overline{\mathrm{dSST_{obs}}}$ north of 60°N, for example in the Arctic Ocean north of Alaska, and the seas surrounding Greenland and Iceland.

The geographical distribution of $\overline{\mathrm{dSST_{mod}}} - \overline{\mathrm{dSST_{obs}}}$ for uncoupled and coupled simulations are shown

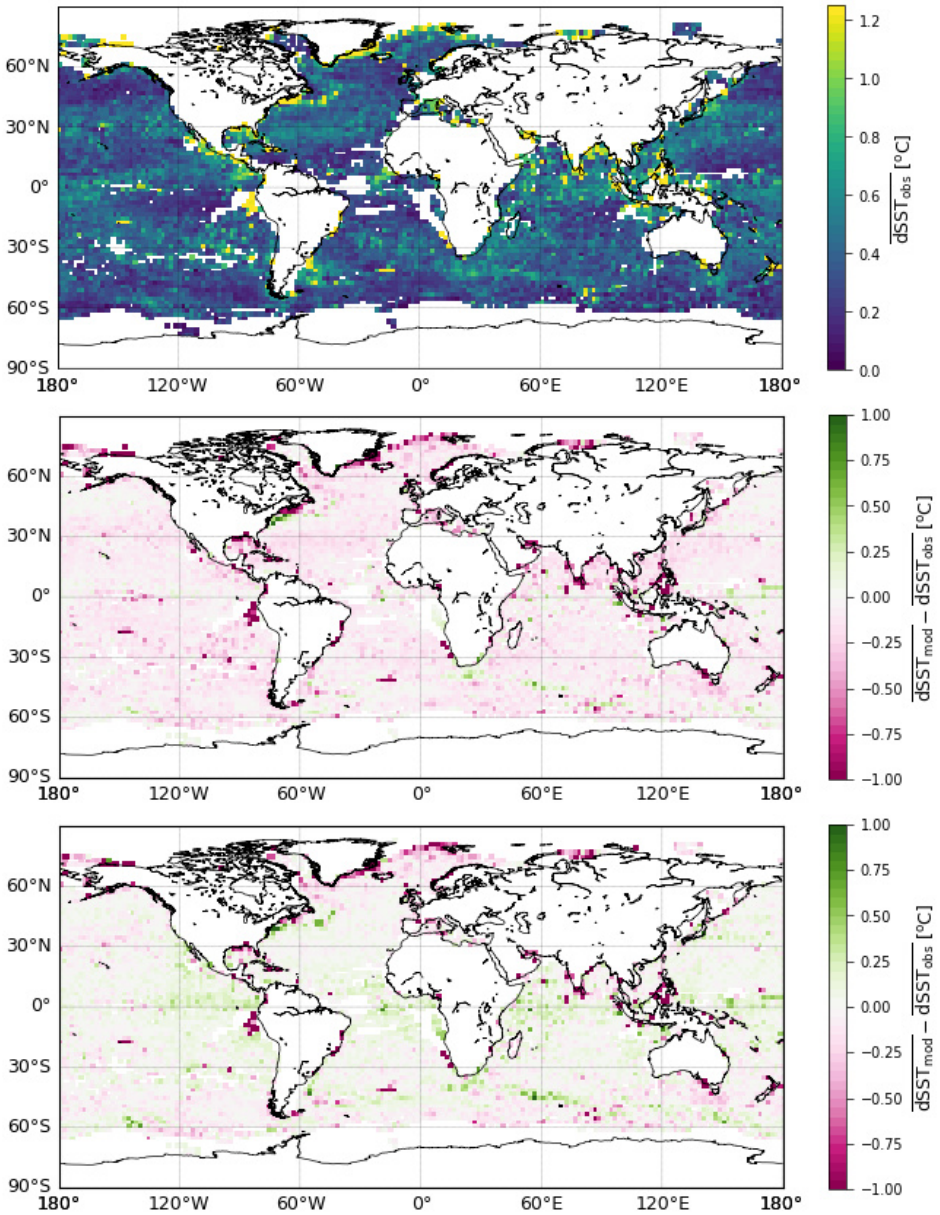

Figure 5: (a) Geographical distribution of $\overline{\mathrm{dSST_{obs}}}$, and the global distribution of $\overline{\mathrm{dSST_{mod}}} - \overline{\mathrm{dSST_{obs}}}$ for each $2^\circ \times 2^\circ$ grid cell for (b) uncoupled and (c) coupled simulations.

in panels (b) and (c), respectively. In the uncoupled simulations, over a large proportion of the globe values are negative (indicating $\overline{\mathrm{dSST_{mod}}} < \overline{\mathrm{dSST_{obs}}}$), and generally less than than -0.3°C. Many of the regions with larger negative values (< -0.5°C), such as waters off the eastern coast of North America, the Indian Subcontinent, and the eastern coast of Greenland, lie close to continental land masses and could be considered as coastal waters.

In the coupled simulations, the general pattern is a shift in $\overline{\mathrm{dSST_{mod}}} - \overline{\mathrm{dSST_{obs}}}$ to higher values, indicating that $\mathrm{dSST_{mod}}$ is on average larger in the coupled simulations than in the uncoupled simulations over much if the ocean, and indeed now larger than $\mathrm{dSST_{obs}}$. Values are positive over much of the tropics, and > 0.5°C in many regions close to the equator. Regions where $\overline{\mathrm{dSST_{mod}}}$ is smaller than $\overline{\mathrm{dSST_{obs}}}$

are mainly confined to higher latitudes, and include areas of the Southern Ocean and the Norwegian and Greenland seas.

5.2 Dependence on key forcing conditions

The diurnal cycle of SST is driven primarily by wind speed and solar insolation—the latter modulated by cloud cover. We next explore the dependence of $\mathrm{dSST_{mod}}$ on the 10-m wind speed (U_{10}) and the total cloud cover (TCC) in both the uncoupled and coupled simulations, and compare with the dependencies of $\mathrm{dSST_{obs}}$. In this analysis, values have been subset into 5° latitudinal bands and then further subset by model estimates for U_{10} or TCC to obtain mean values for each subgroup. Model estimates for U_{10} and TCC were used for consistency, due to the lack of observations of these quantities from many of the observation stations.

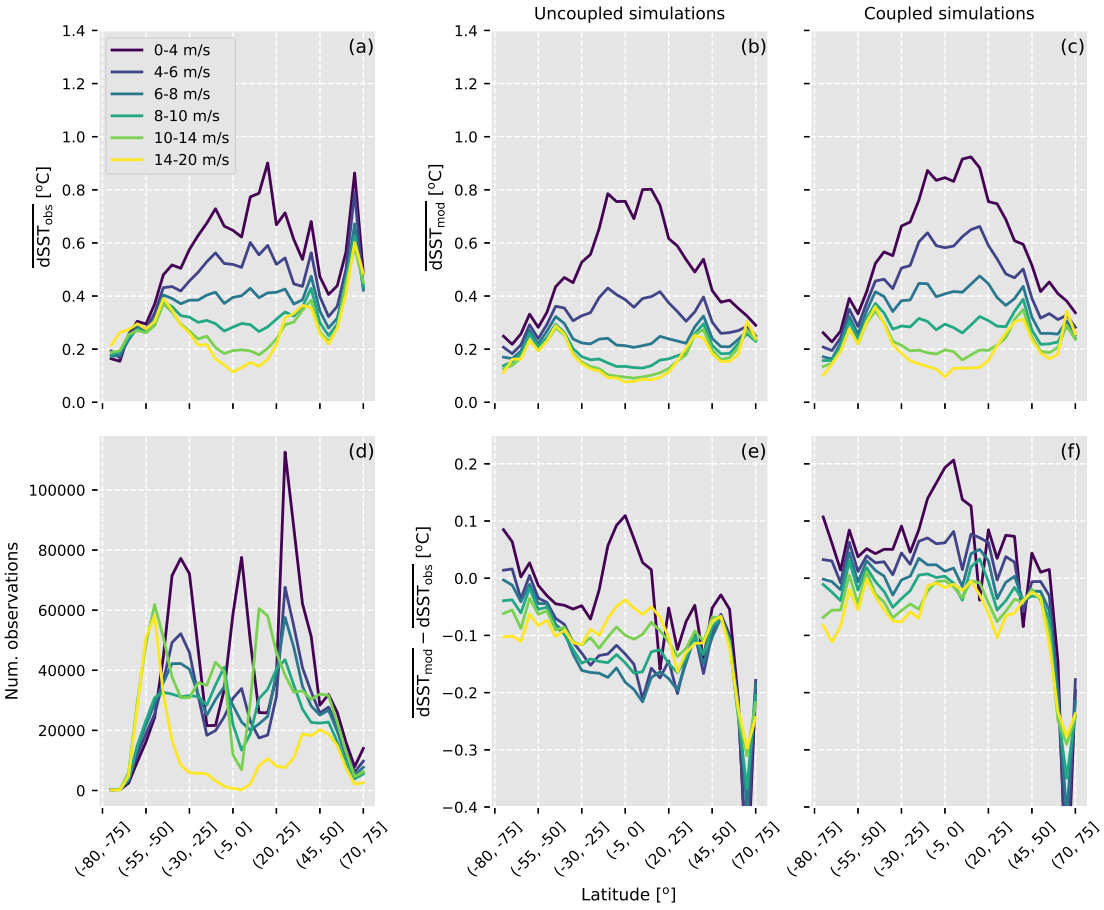

Figure 6: The latitudinal dependence of (a) observed $\overline{\mathrm{dSST_{obs}}}$, (d) the corresponding number of observations, model $\overline{\mathrm{dSST_{mod}}}$ for (b) uncoupled and (c) coupled simulations, and model $\overline{\mathrm{dSST_{skin}}}-$ observed $\overline{\mathrm{dSST_{obs}}}$ for (e) uncoupled and (f) coupled simulations. Estimates are subset by model values for the 10-m wind speed.

Comparing the U_{10} dependence of $\overline{\mathrm{dSST_{mod}}}$ for the uncoupled and coupled experiments with that for $\overline{\mathrm{dSST_{obs}}}$ reveals similarities and differences in behaviour. In the observations, there is a clear pattern of decreasing diurnal cycle amplitude with increasing U_{10} for regions equatorward of approximately

40°N/S. This behaviour is better captured in $\overline{\text{dSST}_{\text{mod}}}$ estimates from the coupled simulations than estimates from uncoupled simulations; in the uncoupled simulations, values of $\overline{\text{dSST}_{\text{mod}}}$ are up to -0.2°C smaller than estimates for $\overline{\text{dSST}_{\text{obs}}}$ at all but the lowest wind speeds. The values of $\overline{\text{dSST}_{\text{mod}}} - \overline{\text{dSST}_{\text{obs}}}$ therefore vary quite significantly with latitude and wind speed in the uncoupled simulations (panel e), whereas the difference is much more uniform in the coupled simulation results, and closer to zero (panel f). For the lowest wind speed range ($U_{10} < 4$ m.s^{-1}) in the equatorial region, model bias increases in the coupled simulations, with overestimation of the diurnal cycle amplitude by up to 0.2°C.

Both model configurations fail to replicate the dependence of the observations on U_{10} in the northern extra-tropics and high latitudes, in particular the local peak in $\overline{\text{dSST}_{\text{obs}}}$ at approximately 40°N and 65°N. Both local maxima show a reduction of the observed diurnal cycle amplitude with increasing wind speed. There is an increase in $\overline{\text{dSST}_{\text{mod}}}$ at these latitudes, but values predicted by the model are underestimated, particularly so for the local peak at 65°N. This leads to large differences between model and observed values of the diurnal cycle amplitude (panels e and f) for both uncoupled and coupled experiments.

The number of observations used to calculate $\overline{\text{dSST}_{\text{obs}}}$ for each wind speed range is shown in panel d. Data sparsity clearly increases towards to poles across the range of wind speeds, and data volume is greatly reduced for the highest wind speed range in the tropics.

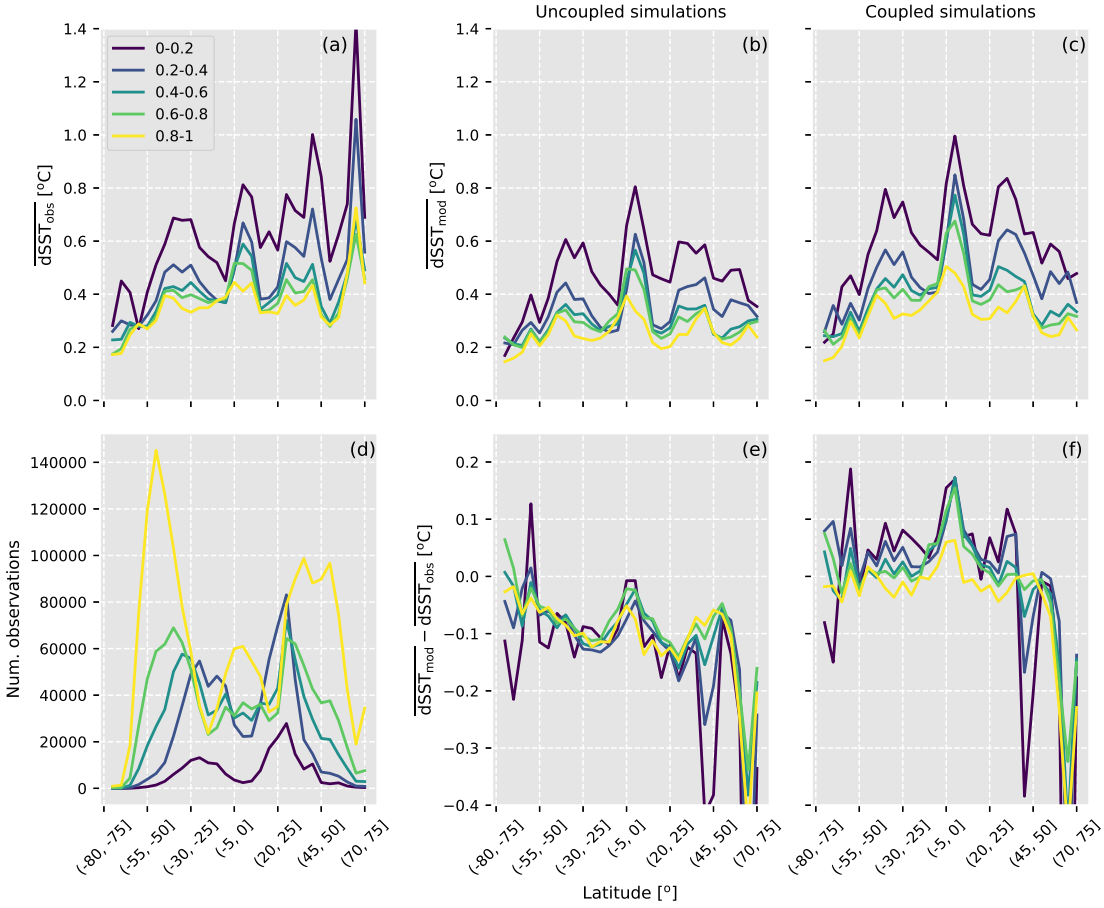

Figure 7: As in Figure 6 but with data subset by total cloud cover.

The latitudinal variation of the dependence of the diurnal cycle amplitude on total cloud cover is explored in Figure 7. The value of $\overline{\text{dSST}_{\text{obs}}}$ generally increases with decreasing cloudiness across the latitudes

(panel a). This dependence is captured reasonably well in both the uncoupled and coupled model results for $\overline{\mathrm{dSST}_{\mathrm{mod}}}$, but—as with results for the U_{10} dependence—there is a clear signal that the diurnal cycle amplitudes of observed SST in the Northern Hemisphere extra-tropics and high latitudes are significantly larger than predictions for $\overline{\mathrm{dSST}_{\mathrm{mod}}}$.

A notable feature distinguishing the behaviour of the two sets of simulations is that $\overline{\mathrm{dSST}_{\mathrm{mod}}}$ is generally larger in the coupled simulations than equivalent values from the uncoupled simulations across all latitudes; this relative increase is generally larger in equatorial regions and when TCC is low. In the uncoupled simulations, the values of $\overline{\mathrm{dSST}_{\mathrm{mod}}} - \overline{\mathrm{dSST}_{\mathrm{obs}}}$ are negative, i.e., $\overline{\mathrm{dSST}_{\mathrm{mod}}}$ is consistently smaller than $\overline{\mathrm{dSST}_{\mathrm{obs}}}$ (panel e). Overall higher values of $\overline{\mathrm{dSST}_{\mathrm{mod}}}$ in the coupled simulations brings values of $\overline{\mathrm{dSST}_{\mathrm{mod}}} - \overline{\mathrm{dSST}_{\mathrm{obs}}}$ closer to zero, especially for extra-tropical regions (panel f). However, the increase in $\overline{\mathrm{dSST}_{\mathrm{mod}}}$ in the coupled simulations increases model–observation difference for latitudes close to the equator under all total cloud cover regimes.

5.3 Diurnal cycle phase

5.3.1 Diurnal cycle phase variation in modelled and observed SST

Analysis of the diurnal cycle phase can give insight into how well the coupled model is representing diurnal variation. In Figure 8 we compare $\mathrm{dSST}_{\mathrm{mod}}$ phase in the uncoupled (left column) and coupled (right column) simulations with $\mathrm{dSST}_{\mathrm{obs}}$ phase, for a subset of days spanning the 10-day forecasts.

Observed diurnal temperature cycle peaks in early afternoon (generally between 12 pm and 4 pm, and centered on 2 pm, LST). In the uncoupled simulations, $\mathrm{dSST}_{\mathrm{mod}}$ phase is slightly displaced from the 1:1 line, with the diurnal cycle reaching its maximum value slightly earlier in the afternoon. In contrast, in the coupled forecasts the diurnal cycle phase is delayed by roughly two hours, and now later in the day than the observed diurnal cycle phase. Based on correlation coefficient values, the diurnal cycle phase of $\mathrm{dSST}_{\mathrm{mod}}$ is closer to that of $\mathrm{dSST}_{\mathrm{obs}}$. However, there remains a not insignificant frequency of occurrence of cases where the diurnal cycle phase in the coupled forecasts is too early or too late in the day.

5.3.2 Latitudinal and seasonal dependence of diurnal cycle phase

We next explore the latitude and seasonal dependence of diurnal cycle phase in the uncoupled and coupled model simulations, with comparison to the dependencies exhibited in the observations (Figure 9). In this analysis, we again investigate the latitudinal dependence through grouping data into 5° latitudinal bands. Results for the four seasons are shown independently.

A general pattern of delayed diurnal cycle phase in the coupled model simulations —with regards to both the uncoupled model predictions and the observations—is evident. The largest discrepancies between the coupled model and the observations occur in the tropics and the northern/southern midlatitudes during their respective summer months; here, the coupled model prediction for $\mathrm{dSST}_{\mathrm{mod}}$ phase is often 60–90 minutes later in the day than the phase of $\mathrm{dSST}_{\mathrm{obs}}$, with the phase in the uncoupled forecasts often 30–90 minutes earlier still. The coupled model predictions for the diurnal cycle phase are closest to observations in the northern/southern mid- to high-latitudes in their respective winter months, with agreement to within 30 minutes. In the Southern Ocean around 40°S both the uncoupled and coupled simulations predict the diurnal cycle phase too early in the day, whilst the opposite is true at approximately 60°N during the Northern hemisphere winter.

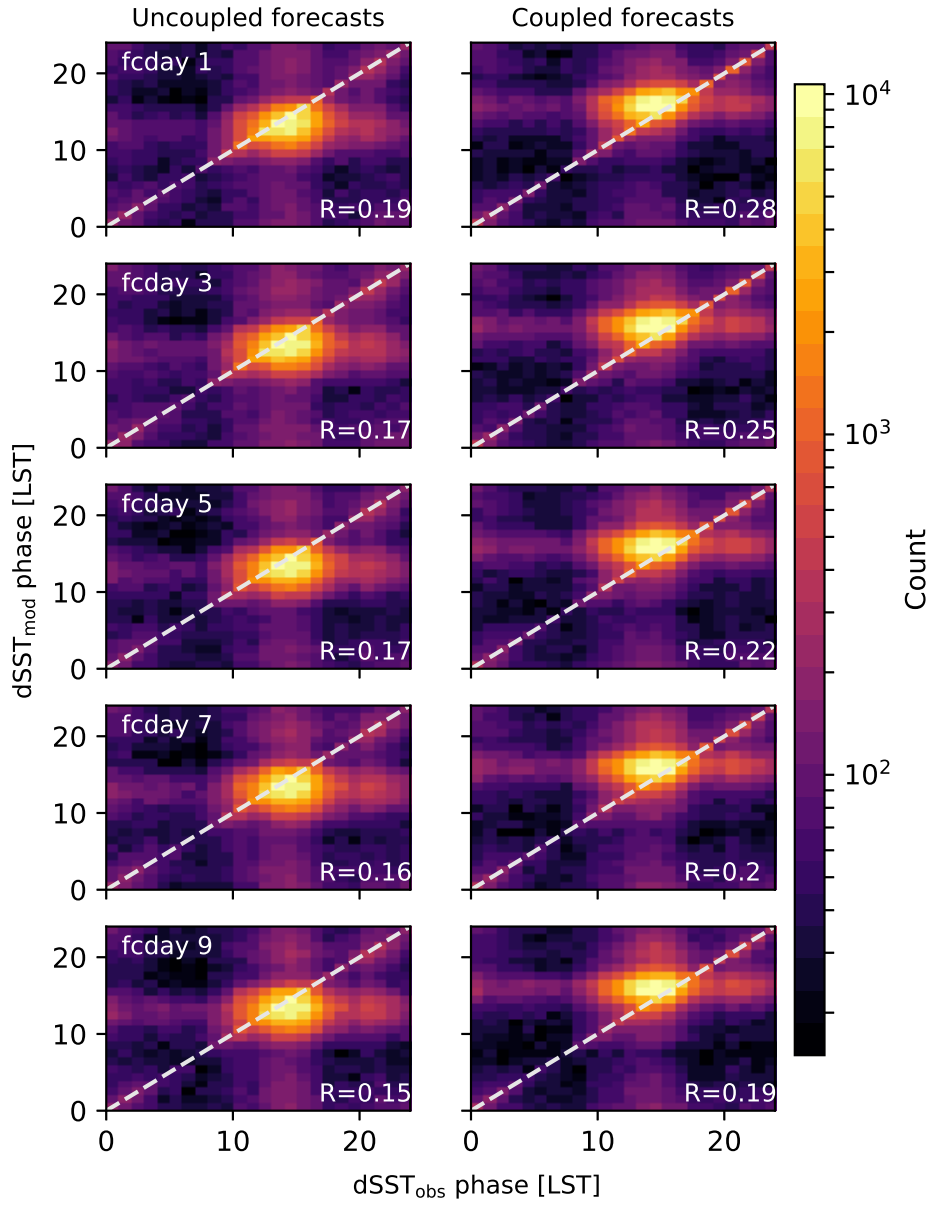

Figure 8: 2D density plots of $dSST_{obs}$ and $dSST_{mod}$ estimates on select days of the forecast validity range for (left column) uncoupled and (right column) coupled simulations.

6 Discussion

A large database of drifting buoy measurements has been used to obtain order 4,775,000 model–observation estimates of diurnal cycle amplitude, enabling verification of the diurnal cycle of SST in the IFS model in uncoupled and coupled configurations. Model predictions have been compared to observed values obtained from buoys and moored arrays with a depth of measurement of roughly 20–30 cm. This distinction likely introduce some variability into the results, which cannot be fully accounted for. But while diurnal cycle characteristics of the skin and at-depth SST may vary under specific meteorological and oceanic conditions, given the volume of data used in this study, it is not expected that this factor affects

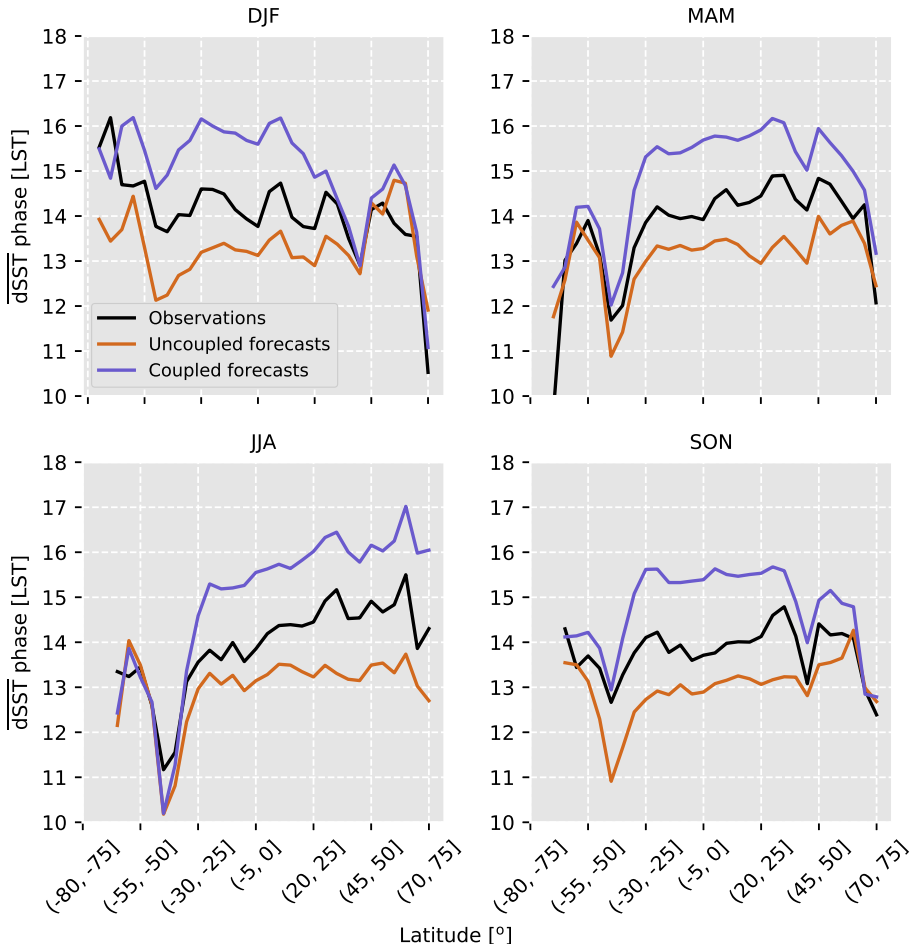

Figure 9: The latitudinal dependence of observed $\overline{\mathrm{dSST}_{\mathrm{obs}}}$ phase (black line) and model $\overline{\mathrm{dSST}_{\mathrm{mod}}}$ phase for uncoupled (brown line) and coupled (blue line) simulations for (a) December–February, (b), March–May, (c) June–August, and (d) September–October.

conclusions from the analyses.

Diurnal cycle amplitude has been estimated using the maximum and minimum values of SST during consecutive 24-hr periods of each 10-day forecast. This method therefore accounts for all factors that impart variability into SST, including mechanisms not directly related to solar insolation-driven diurnal warming—for example, through advection of warmer water in the vicinity of the observation platform, or via wind-induced mixing of surface waters. Diurnal cycle phase has been estimated using the maximum value of SST during consecutive 24-hr periods of each 10-day forecast. When the diurnal cycle in SST is weak, the phase may be ambiguous. We have thus calculated the phase only when the diurnal cycle amplitude exceeds a set threshold (0.25°C).

Differences between modelled and observed SST diurnal cycle amplitude are reduced in coupled forecasts; this is a result of an overall increase in diurnal cycle amplitude in the coupled simulations, compared with uncoupled simulations. However, there remain regions where coupled model predictions of the diurnal cycle amplitude show sizeable bias against observations, with many of these regions showing similar bias to those in the uncoupled forecasts. In particular, coupled model predictions for $\mathrm{dSST}_{\mathrm{mod}}$ are overestimated in regions of the ocean close to the equator, and $\mathrm{dSST}_{\mathrm{mod}}$ is consistently underpre-

dicted in the northern high latitudes. The latter, however, may be a result of observational biases within the data set, as the observed values for the diurnal cycle amplitude are significantly larger than would be expected.

Despite utilising a year's worth of in situ data obtained across the global ocean, there remain regions where measurements are not taken, and individual stations that report suspect data or measure too infrequently to calculate diurnal variation. Data sparsity at high latitudes (northwards of 65°N and southward of 65°S) is also an issue. Our analyses reveal larger differences between $\mathrm{dSST}_{\mathrm{mod}}$ and $\mathrm{dSST}_{\mathrm{obs}}$ in northern high latitudes; these differences are not generally reduced in the coupled simulations.

The observed dependence of SST diurnal cycle amplitude on total cloud cover and the 10-m wind speed is better replicated in coupled forecasts. In particular, the diurnal cycle amplitude in coupled forecasts is more in line with the observed amplitude in regions equatorward of 40°N/S; this is the case over the range of wind speeds. However, there still exists quite significant differences between model and observed behaviour, particularly at northern high latitudes where the mean difference between $\mathrm{dSST}_{\mathrm{obs}}$ and $\mathrm{dSST}_{\mathrm{mod}}$ can exceed 0.4°C under comparable wind speeds or cloud cover. Investigating the dependence of diurnal cycle amplitude on U_{10} reveals local peaks (at approximately 45°N and 65°N) in observed values that aren't well captured in either the uncoupled or coupled simulations. It is not known at this stage if these anomalously large values are real features, or are instead the result of measurement errors from a set of observation stations. However, these features seem robust across the wind speed range, with diurnal cycle amplitude larger under lower wind speeds, as expected. One limitation of this analysis is that model values for U_{10} and TCC were used in lieu of observed values, which are not reported by the majority of stations. However, the systematic difference between $\mathrm{dSST}_{\mathrm{obs}}$ and $\mathrm{dSST}_{\mathrm{mod}}$ cannot be explained by potential errors in model values for U_{10} and TCC.

The skill in forecasting diurnal cycle phase is marginally improved in the coupled model. There is however evidence that the phase of the diurnal cycle is delayed in the coupled model with respect to the observed phase. Indeed, averaged over all observations, the size of this phase shift seems to correspond with the amplitude of the diurnal cycle. This finding could be explored in more detail by focusing on individual case studies, to explore for example whether the ocean model's uppermost layer is too slow to warm. Having a thinner more responsive top layer in the ocean model might also change the phase of the maximum to earlier in the solar day.

7 Conclusions

We have investigated the diurnal cycle of SST in uncoupled and coupled 10-day forecasts with the ECMWF model. Model predictions for the amplitude of the diurnal cycle of SST have been compared with estimates from in situ observations, and the dependence of the diurnal cycle amplitude on important forcings—namely the 10-m wind speed and total cloud cover—has been explored. The modelled phase of the diurnal cycle has also been compared with the observed phase.

Averaged over the set of 10-day simulations, and over the global ocean, the SST diurnal cycle amplitude in the uncoupled simulations is around one tenth of a degree smaller than that for the observed SST. In coupled simulations, the diurnal cycle amplitude is on average larger and consistently within a few tenths of a degree of observed values. This leads to a higher degree of correlation with observations for the coupled model. Despite this, the frequency of occurrence of larger discrepancies between model and observed diurnal cycle amplitude—i.e., a difference with magnitude greater than 1°C—remains similar between the two model implementations.

The coupled model simulations better replicate the dependence of diurnal cycle amplitude on the 10-m wind speed. The dependence of observed diurnal cycle amplitude on total cloud cover is also better replicated by the coupled simulations, with smaller differences between observed diurnal cycle amplitude and model estimates under most conditions. The results of this study indicate that a coupled implementation of the IFS model can accurately simulate diurnal variation in SST, at least as well as the uncoupled configuration. However, our results reveal inherent biases in predicting SST diurnal cycle statistics that remain despite use of an interactive ocean.

On average, SST diurnal cycle phase is shifted later in the day in the coupled configuration. This shift brings the coupled model results closer in line with the observations, but the phase is systematically delayed with respect to the observations, often by 60–90 minutes. This delayed phase is most evident under conditions when the diurnal cycle amplitude would be expected to be large.

This work is preparatory for further sensitivity experiments exploring model representation of the physical mechanisms at the ocean surface that drive the diurnal cycle. This work could also be extended by using satellite measurements of skin SST to verify modelled diurnal cycle of SST. Though use of satellite data brings its own challenges in obtaining model-observation matchups with adequate temporal and spatial resolution, such data provides further means of validating model predictions.

References

Bernie, D. J., Guilyardi, E., Madec, G., Slingo, J. M., and Woolnough, S. J. (2007). Impact of resolving the diurnal cycle in an ocean–atmosphere GCM. Part 1: a diurnally forced OGCM. *Climate Dynamics*, 29(6):575–590.

Bernie, D. J., Guilyardi, E., Madec, G., Slingo, J. M., Woolnough, S. J., and Cole, J. (2008). Impact of resolving the diurnal cycle in an ocean–atmosphere GCM. Part 2: A diurnally coupled CGCM. *Climate Dynamics*, 31(7-8):909–925.

Brassington, G., Martin, M., Tolman, H., Akella, S., Balmeseda, M., Chambers, C., Chassignet, E., Cummings, J., Drillet, Y., Jansen, P., Laloyaux, P., Lea, D., Mehra, A., Mirouze, I., Ritchie, H., Samson, G., Sandery, P., Smith, G., Suarez, M., and Todling, R. (2015). Progress and challenges in short- to medium-range coupled prediction. *Journal of Operational Oceanography*, 8(sup2):s239–s258.

Breivik, Ø., Mogensen, K., Bidlot, J.-R., Balmaseda, M. A., and Janssen, P. A. E. M. (2015). Surface wave effects in the NEMO ocean model: Forced and coupled experiments. *Journal of Geophysical Research: Oceans*, 120(4):2973–2992.

Brunke, M. A., Zeng, X., Misra, V., and Beljaars, A. (2008). Integration of a prognostic sea surface skin temperature scheme into weather and climate models. *Journal of Geophysical Research: Atmospheres*, 113(D21).

Dai, A. and Trenberth, K. E. (2004). The diurnal cycle and its depiction in the community climate system model. *Journal of Climate*, 17(5):930–951.

Donlon, C., Minnett, P., Gentemann, C., Nightingale, T., Barton, I., Ward, B., and Murray, M. (2002). Toward improved validation of satellite sea surface skin temperature measurements for climate research. *Journal of Climate*, 15(4):353–369.

Donlon, C., Rayner, N., Robinson, I., Poulter, D. J. S., Casey, K. S., Vazquez-Cuervo, J., Armstrong, E., Bingham, A., Arino, O., Gentemann, C., May, D., LeBorgne, P., Piollé, J., Barton, I., Beggs, H., Merchant, C. J., Heinz, S., Harris, A., Wick, G., Emery, B., Minnett, P., Evans, R., Llewellyn-Jones, D., Mutlow, C., Reynolds, R. W., and Kawamura, H. (2007). The global ocean data assimilation experiment high-resolution sea surface temperature pilot project. *Bulletin of the American Meteorological Society*, 88(8):1197–1213.

Donlon, C. J., Martin, M., Stark, J., Roberts-Jones, J., Fiedler, E., and Wimmer, W. (2012). The operational sea surface temperature and sea ice analysis (OSTIA) system. *Remote Sensing of Environment*, 116:140–158.

Fairall, C. W., Bradley, E. F., Godfrey, J. S., Wick, G. A., Edson, J. B., and Young, G. S. (1996). Cool-skin and warm-layer effects on sea surface temperature. *Journal of Geophysical Research: Oceans*, 101(C1):1295–1308.

Filipiak, M. J., Merchant, C. J., Kettle, H., and Borgne, P. L. (2012). An empirical model for the statistics of sea surface diurnal warming. *Ocean Science*, 8(2):197–209.

Johnson, R. H., Rickenbach, T. M., Rutledge, S. A., Ciesielski, P. E., and Schubert, W. H. (1999). Trimodal characteristics of tropical convection. *Journal of Climate*, 12(8):2397–2418.

Kawai, Y. and Wada, A. (2007). Diurnal sea surface temperature variation and its impact on the atmosphere and ocean: A review. *Journal of Oceanography*, 63(5):721–744.

Madec, G. (2008). *NEMO ocean engine*. Note du Pôle de modélisation, Institut Pierre-Simon Laplace (IPSL), France, No 27, ISSN No 1288-1619.

McLay, J. G., Flatau, M. K., Reynolds, C. A., Cummings, J., Hogan, T., and Flatau, P. J. (2012). Inclusion of sea-surface temperature variation in the U.S. Navy ensemble-transform global ensemble prediction system. *Journal of Geophysical Research: Atmospheres*, 117(D19).

Mogensen, K., Keeley, S., and Towers, P. (2012). Coupling of the NEMO and IFS models in a single executable. Technical Memorandum 673, ECMWF.

Mogensen, K. S., Magnusson, L., and Bidlot, J.-R. (2017). Tropical cyclone sensitivity to ocean coupling in the ECMWF coupled model. *Journal of Geophysical Research: Oceans*, 122(5):4392–4412.

Soloviev, A. and Lukas, R. (1997). Observation of large diurnal warming events in the near-surface layer of the western equatorial pacific warm pool. *Deep Sea Research Part I: Oceanographic Research Papers*, 44(6):1055–1076.

Soloviev, A., Lukas, R., Soloviev, A., and Lukas, R. (2013). *The Near-Surface Layer of the Ocean*. Springer Netherlands.

Stuart-Menteth, A. C. (2003). A global study of diurnal warming using satellite-derived sea surface temperature. *Journal of Geophysical Research*, 108(C5).

Takaya, Y., Bidlot, J.-R., Beljaars, A. C. M., and Janssen, P. A. E. M. (2010a). Refinements to a prognostic scheme of skin sea surface temperature. *Journal of Geophysical Research*, 115(C6).

Takaya, Y., Vitart, F., Balsamo, G., Balmaseda, M. A., Leutbecher, M., and Molteni, F. (2010b). Implementation of an ocean mixed layer model in IFS. Technical Memorandum 622, ECMWF.

Ward, B. (2006). Near-surface ocean temperature. *Journal of Geophysical Research*, 111(C2).

Webster, P. J., Clayson, C. A., and Curry, J. A. (1996). Clouds, radiation, and the diurnal cycle of sea surface temperature in the tropical western pacific. *Journal of Climate*, 9(8):1712–1730.

Woolnough, S. J., Vitart, F., and Balmaseda, M. A. (2007). The role of the ocean in the Madden–Julian Oscillation: Implications for MJO prediction. *Quarterly Journal of the Royal Meteorological Society*, 133(622):117–128.

Zeng, X. and Beljaars, A. (2005). A prognostic scheme of sea surface skin temperature for modeling and data assimilation. *Geophysical Research Letters*, 32(14).

Zeng, X. and Dickinson, R. E. (1998). Impact of diurnally-varying skin temperature on surface fluxes over the tropical pacific. *Geophysical Research Letters*, 25(9):1411–1414.

Zuo, H., Balmaseda, M. A., and Mogensen, K. (2017). The new eddy-permitting ORAP5 ocean reanalysis: description, evaluation and uncertainties in climate signals. *Climate Dynamics*, 49(3):791–811.

Zuo, H., Balmaseda, M. A., Mogensen, K., and Tietsche, S. (2018). OCEAN5: the ECMWF Ocean Reanalysis System ORAS5 and its real-time analysis component. Technical Memorandum 823, ECMWF.

Data availability

The data used to produce the diagnostics of this ECMWF Technical Memorandum can be obtained from the authors upon requests.